Adhesion of electrolessly deposited Ni(P) layers on alumina ceramic. I. Mechanical properties.

Adhesion of electrolessly deposited Ni(P) layers on alumina ceramic. I. Mechanical properties

J. W. Severin, R. Hokke, and G. de With
Philips Research Laboratories, P.O. Box 80 000, 5600 JA Eindhoven, The Netherlands

(Received 29 October 1992; accepted for publication 29 November 1993)

The adhesion mechanism of electrolessly deposited Ni(P) on alumina ceramic substrates has been investigated. The adhesion was measured by direct pull-off tests and by 90° peel tests, which provided information on adhesion strength and fracture energy, respectively. An assessment is made of quantitative aspects of both adhesion measurement techniques. The observed mechanical behavior is rationalized using the Griffith–Irwin theory. Two types of alumina substrates with different roughnesses were used. Ni(P) was deposited from two types of electroless Ni(P) solutions, one with glycine and one with acetate as the complexing agent. The fracture surfaces were analysed with scanning electron microscopy, combined with energy dispersive analysis of x rays. The adhesion strength of the glycine-type Ni(P) was much higher and the fracture energy was lower than that of the acetate-type Ni(P), for both substrate types. This implies that the difference in adhesion strength is not caused by differences in interfacial chemical bonding, but rather by differences in flaw sizes. Since high adhesion strength was measured on smooth substrates, along with low peel strength, it is concluded that strong adhesion can be obtained without making use of mechanical interlocking. Further research should be aimed at controlling the interfacial flaw sizes.

I. INTRODUCTION

A. Aim

The metallization of alumina ceramic surfaces with electroless Ni(P) is often used in the electronics industry, among other things for integrated circuit (IC) packaging, and printed circuit and sensor applications.[1–5] Generally, the adhesion between electroless nickel layers and nonconducting substrates such as polymers, glass, and ceramics, is weak. Various studies have been devoted to the optimization of process parameters with respect to the adhesion strength of Ni(P) on alumina.[1–6] The adhesion strength is generally found to be most strongly influenced by etching conditions, while nucleation and metallization conditions are only of secondary importance. According to most authors, this suggests that the adhesion is determined by mechanical interlocking interactions.[7] However, for theoretical reasons adhesion strength data are insufficient for obtaining conclusive information on microscopic interfacial interactions as described in Sec. II. Moreover, very few interface and fracture surface analyses are reported in these literature references.

B. Methods

In this work a different approach is followed in order to gain insight into the backgrounds of the adhesion of both types of Ni(P) on alumina. In order to vary the contribution of mechanical interlocking to the adhesion, two types of substrates with different roughnesses are used, further denoted as rough- and smooth-type substrates. In addition, two types of electroless metallization solutions are used, one with acetate as the complexing agent and one with glycine. The corresponding deposits are denoted by acetate and glycine-type Ni(P), respectively. Information on adhesion strength, which is influenced by extrinsic factors such as interfacial flaws,[8,9] is combined with information on the interfacial fracture energy, which is mainly determined by intrinsic factors such as interface chemical bonding or mechanical interlocking. For the adhesion strength measurements the direct pull-off (DPO) test is used[1–6,10–13] and for the fracture energy measurement the peel test is used. The fracture surfaces are analyzed on micrometer scale with a scanning electron microscope (SEM), equipped with energy-dispersive analysis of x rays (EDX). A more detailed study on the structure and chemistry of the interface and the fracture surfaces of the sample types used in the present investigation is reported in an accompanying article.[14]

C. Preface

The following theoretical section deals with backgrounds of adhesion strength and adhesion measurements. In the third, experimental, section first the sample preparation is described, followed by methods for the characterization of adhesion strength and fracture energy. In the fourth section the results of this set of analyses are reported. The last sections deal with a discussion of the results and conclusions.

II. THEORY

This section deals with theoretical backgrounds of the adhesion strength and fracture energy measurements. In addition, a statistical method for interpretation of the adhesion strength data, i.e., Weibull statistics, is discussed.

 0021-8979/94/75(7)/3402/12/$6.00

A. Adhesion strength

The adhesion strength σ_f is determined by, among other factors, the fracture energy G_c and the critical flaw size a_{cr} and is usually described by the Griffith–Irwin relation:[15–17]

$$\sigma_f^2=\frac{KEG_c}{a_{cr}}, \tag{1}$$

where K is a geometric factor and E is Young's modulus. The fracture energy G_c is formed by an intrinsic fracture energy term G_i and a contribution from plastic deformation of material at the crack tip G_{pl},

$$G_c=G_i+G_{pl}. \tag{2}$$

The intrinsic fracture energy is the energy required for example to overcome van der Waals forces and to break chemical bonds. The order of magnitude of G_i is 0.01–0.1 J/m^2 for van der Waals interactions and 0.5–5 J/m^2 for chemical bonds. During fracture, stresses are near to the theoretical strength at the crack tip. This causes plastic deformation in the metal layer during fracture, represented by G_{pl}. Since the stresses at the crack tip depend on the strength of the interfacial bonds, G_{pl} depends on G_i, and therefore Eq. (2) can be written as[18]

$$G_c=f_l G_i, \tag{3}$$

in which f_l is the energy-loss factor. For purely brittle fracture, such as with ceramics at low temperature, plastic deformation does not play a role and f_l is slightly larger than unity for smooth fracture planes. For metal layers on ceramics G_c values of the order of 100 J/m^2 are found,[19] which means that f_l is 10–100. For polymers on rigid substrates these values are of the order of 1000 for G_c,[20] and thus 100–1000 for f_l.

From this relation it is clear that in order to evaluate the influence of interface chemistry on adhesion strength, the fracture energy must be measured separately. This is done by the peel test. Conditions under which the peel test can be used for a quantitative fracture energy measurement are considered.

B. Peel test

The peel test has often been used for measuring adhesion,[21,22] both of metal films[23] and polymer films.[24,25] In the 90° peel test the peel force is measured as a function of displacement, as shown in Fig. 1. The peel energy G_p is obtained by the following expression:

$$G_p=\frac{F_p\Delta L}{\Delta A}=\frac{F_p}{W}, \tag{4}$$

in which F_p is the peel force, ΔL is the peeled length, ΔA is the peeled area, and W is the width of the peel strip. For this measurement the following energy balance can be used:

$$G_p=G_c+G_{def}-G_{el}. \tag{5}$$

During peeling energy is consumed by fracture G_c and possibly by bulk plastic deformation of the film G_{def}, while

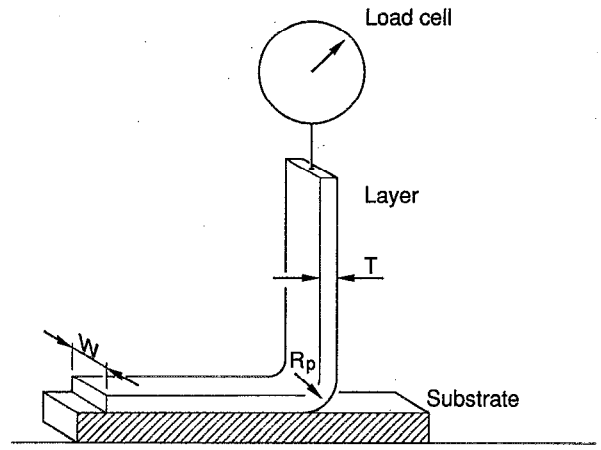

FIG. 1. Schematic presentation of peel test. The symbols W, T_l, and R_p denote the width of the peel strip, the thickness, and the peel radius, respectively.

energy is supplied externally by peeling G_p and internally by relaxation of residual stresses in the film G_{el}. All energy terms are per unit area. Note the difference between G_{def} and G_{pl}. The first term stands for bulk plastic deformation in the metal layer, whereas the second term denotes the plastic deformation in the microscopic crack tip zone. These two terms may become indistinguishable when the size of the plastic zone is of the order of the layer thickness. If no energy is lost in bulk plastic deformation of the metal layer and if the residual strain energy in the layer is very small, then the peel energy equals the fracture energy.

The residual strain energy G_{el} can either be caused by the deposition process as built-in stresses or by a difference in thermal expansion between layer and substrate. The amount of elastic strain energy U per unit volume V due to the difference in thermal expansion is given by

$$\frac{U}{V}=\int_0^{\epsilon_T}\sigma\,d\epsilon=E\int_0^{\epsilon_T}\epsilon\,d\epsilon=\frac{E\epsilon_T^2}{2}=\frac{E(\Delta\alpha\Delta T)^2}{2}, \tag{6}$$

in which σ is the stress, E is the Young's modulus of the film, Δa is the difference in thermal-expansion coefficients, and ΔT is the temperature difference. This can be expressed in elastic strain energy per unit area if the volume V is equal to area A times layer thickness T_l,

$$G_{el}=\frac{ET_l(\Delta\alpha\Delta T)^2}{2}. \tag{7}$$

In a similar manner as with Eq. (6), with Eq. (8) the residual strain energy G_{el} due to built-in stresses can be calculated if the amount of internal stress σ_i is known,

$$\frac{G_{el}}{T_l}=\frac{\sigma_i^2}{2E}. \tag{8}$$

C. Weibull statistics

Weibull[26] suggested that strength data could be fitted with Eq. (9a),

$$P_f=1-e^{-[(\sigma_f-\sigma_u)/\sigma_0]^m}. \tag{9a}$$

Here P_f is an estimate of the failure probability, σ_f is the adhesion strength, σ_0 is a normalization constant, σ_u is a threshold stress value below which no fracture occurs, usually taken as zero, and m is a fit parameter called the Weibull modulus. An estimation of P_f can be made by placing the experimental strength values in the order of increasing strength. The failure probability P_f can then be estimated by[27]

$$P_f=\frac{i}{N+1} \tag{10a}$$

or

$$P_f=\frac{i-0.5}{N}, \tag{10b}$$

in which N is the number of test specimens and i is the rank number of a particular specimen in the series of measurements. Recent computer simulations have shown that Eq. (10b) is more appropriate, i.e., yields the most accurate estimate with the least bias.[27] Initially, Weibull statistics were used for the interpretation of bulk material strength data, but later it was also used for adhesion strength.[9]

Equation (9a) can be rewritten as ($\sigma_u=0$)

$$\ln[-\ln(1-P_f)]=m\ln\sigma_f-m\ln\sigma_0. \tag{9b}$$

By plotting $\ln[-\ln(1-P_f)]$ vs $\ln\sigma_f$ a straight line is obtained with slope m, if a single distribution of flaw types is present. At $\sigma_f=\sigma_0$, failure occurs with 63% probability. Hence, the measurement results can be described by two parameters m and σ_0 in which m is a measure of scatter and σ_0 is a measure of location. For a large value of m, a small variation in strength values is obtained.

III. EXPERIMENTAL PROCEDURES

In this section the experimental procedures are described for the sample preparation, adhesion measurements, and SEM/EDX fracture surface analyses.

A. Sample preparation

For the sample preparation two types of alumina were used as substrates. The first type was a 96% pure alumina (Hoechst Rubalit 708) with a surface roughness characterized by an R_a value of 0.3 μm as measured with a Tencor α-step step profiler with a tip radius of 2 μm. The second phase was a grain-boundary glass phase, used as a sintering aid. The grain size was of the order of 5 μm as visually estimated. The second substrate (MRC-996) was a 99.5% pure alumina with an R_a value of 0.06 μm and a grain size of the order of 1–2 μm. The additive in this material was mainly MgO. The x-ray-diffraction pattern of the substrate surfaces showed no preferential orientation of the alumina grains. An impression of the surface topography is given by the SEM micrographs of the sintered surfaces of both substrate types described in Sec. IV C. Samples were prepared by first depositing an electroless Ni(P) layer of about 0.3 μm thickness and subsequently electrodepositing a thicker Ni layer from a low-stress sulphamate bath.[28] The internal stress in the sulphamate nickel deposits was measured using a deposit stress analyzer[29] and it was found to amount to 40 MPa. For the adhesion strength test samples, a Ni layer thickness of 2–3 μm was used and for the peel test samples this was about 7 μm.

Prior to the electroless deposition, the alumina plates were first cleaned by immersion in a fluorinated alkylsulphonate detergent solution, then etched in a HF solution and subsequently activated by a standard Sn, Ag, Pd procedure as described in Ref. 30. For the 96% alumina substrates, etching removed the grain-boundary glass phase from the surface of the alumina grains and from regions between surface grains. For the smooth substrates no effect of etching on the surface structure has been observed. The glycine-containing electroless metallization solution only contained three compounds: NaH_2PO_2, $NiCl_2\cdot 6H_2O$, and $HOOC\text{-}CH_2\text{-}NH_2$ in amounts of 10, 30, and 30 g/ℓ respectively. The acetate-containing solution was based on the commercially available Enlyte 512 from OMI. Ni layer thicknesses were measured using a Fisherscope x-ray fluorescence coating thickness meter. The adhesion strength test samples were obtained by breaking metallized plates into pieces of about 6×6 mm^2. For reasons to be explained later, for a number of these measurements the test samples were numbered before breaking.

B. Analyses

1. Adhesion measurements: Strength

The adhesion strengths were measured by the direct pull-off (DPO) test,[10–13,17] as schematically depicted in Fig. 2. An aluminum pull stud (QUAD Sebastian) was bonded with an epoxy adhesive to the metallized ceramic surface by heating for 1 h at 160 °C and the force at which fracture occurs at the metal-ceramic interface was measured using a testing machine (ELE 205) at a cross-head speed of 0.5 mm/min in air atmosphere. All adhesion measurements were performed at room temperature (21 $\pm$2 °C). In Fig. 3 a pull stud bonded on a test sample is shown. Cross sections of such an assembly are shown in Figs. 4(a) and 4(b). The diameter of the bonded area was 2.5 mm, the height of the studs was 12.5 mm, and the angle between nail head and shank of the stud was 140°. The thickness of the adhesive layer varied between 2 and 10 μm and no interfacial voids were observed. At the edge of the stud an adhesive spew fillet of about 0.1 mm was formed. For each strength measurement about 40 data were fitted using Weibull statistics with a computer program of Dortmans and de With.[27] For estimation of P_f Eq. (10b) was used, while for the strength the nominal value given by the pull-off force divided by the bonded area under the stud was used.

2. Adhesion measurements: Fracture energy

The fracture energy was measured using the 90° peel test at a test rate of 1 mm/min in air. In Fig. 1 the peel-test setup is schematically depicted. A 1 N load cell was used and the overall measuring accuracy was $<1\%$. The metal strips were cut with a razor blade to a length of about 50

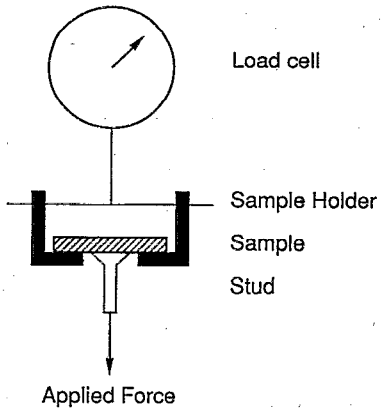

FIG. 2. Schematic presentation of direct pull-off test.

mm and a width W of 15 mm. Peel radii were measured by means of a video camera both during (R_p) and after (R_p') peeling. Initially, a frictionless air bearing was used to keep the peel front exactly below the load cell; however, in later experiments it turned out that the small deviation from 90° (within 5°), made by peeling from a fixed substrate, did not significantly influence the peel energy value. In order to obtain comparable results all peel-test samples received the same thermal treatment as the DPO test samples.

IV. RESULTS

A. Adhesion strength

The results of the DPO adhesion strength measurements are given in Table I. In Figs. 5(a)–5(d) the Weibull plots of these measurements data are shown. The Weibull modulus m and the Weibull normalization constant σ_0 are also listed in Table I.

The strongest adhesion is measured with the glycine-type Ni(P) on the smooth substrates, whereas the weakest adhesion is found with the acetate-type Ni(P) on the same substrates. It is remarkable that the adhesion of the glycine-type Ni(P) on the smooth substrates is even stronger than on the rough substrates. The differences in adhesion strength are significant and reproducible. The Weibull moduli from the samples with glycine Ni(P) are higher than those from the corresponding acetate-type samples. These observations are discussed in Sec. V C.

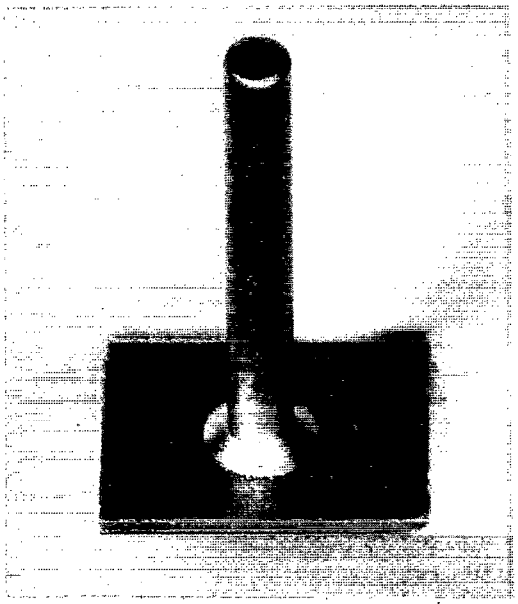

FIG. 3. Pull stud on a metallized rough-type sample.

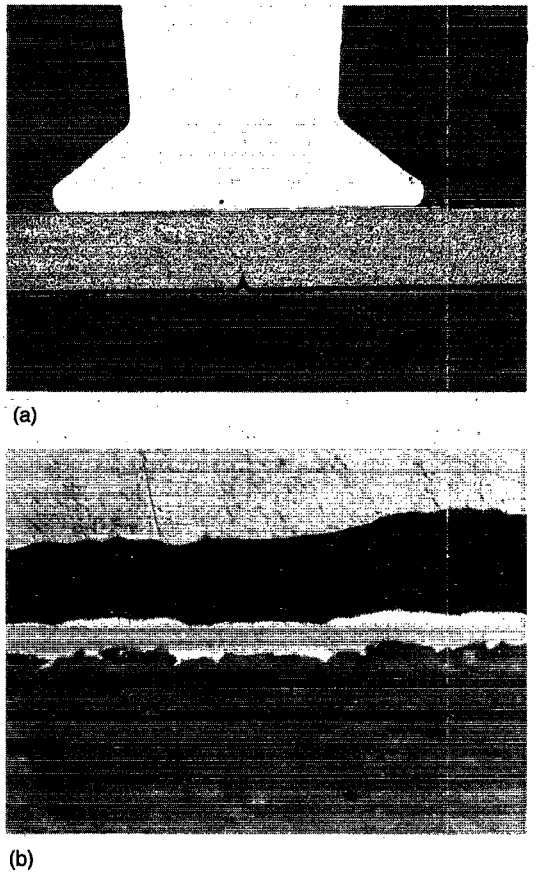

FIG. 4. (a) Optical micrograph of a cross section of a pull stud on a metallized rough-type alumina sample, magnification 32×; (b) sample of (a), magnification 1600×.

In order to identify the original location of the samples on the plates, the test samples on the metallized plates were numbered before breaking. No systematics were detected in the distribution of strong and weak samples over the plates. Moreover, the adhesion strength was found to be independent of the layer thickness, within the investigated range of 0.5–8 μm.

B. Fracture energy

In Figs. 6(a) and 6(b) two typical peel curves are shown for the acetate and the glycine-type samples, respectively. The two layer types show a different experimental behavior in the peel test. Despite the constant displacement rate, the acetate-type Ni(P) always peels in small, rapidly

repeating steps smaller than 0.1 mm. This results in the broad line in the peel plot due to a compressed sawtooth structure of the force-time plot. The glycine-type Ni(P) peels off more continuously and the variation in peel force is mainly caused by buckling of the edges of the metal strip. The physical cause of the difference in peel behavior is unclear. In Table II the results of the peel measurements are listed.

In Fig. 7 the peel energies are plotted against layer thickness with values ranging from 2 to 9 μm of the glycine-type Ni(P) on the smooth alumina substrates. The points are mean values of three to four measurements, except for the two points at the middle, which are both from one measurement. For standard deviations, see Table II.

As described in Sec. III, the adhesion measurements were done in ambient atmosphere. When, however, dry nitrogen was passed over the peel front of the test sample, the peel energy immediately increased by about 10%–20% for all sample types. When the nitrogen flow is stopped, the peel force immediately drops to the original level. A similar decrease is observed when air saturated with water is passed over the peel front. These results show that the peel energy depends on the humidity of the ambient atmosphere. When peeling is stopped, a relaxation effect is observed. When, during this relaxation in normal air, humid air is passed over the sample, the peel force drops to the corresponding level. After switching back to normal air a small increase in peel load is observed. This latter effect can only be explained by partial closure of the crack at the peel front since this whole process occurs at zero peel rate.

In Table III the peel radius of the metal film R_p (see also Fig. 1) is listed for samples with various layer thicknesses. This radius gives information on the relative amount of plastic deformation of the film during peeling. In addition, the radius of the metal film after peeling and at

TABLE I. Adhesion strength data measured by the DPO test. σ_f denotes the mean adhesion strength, s_{n-1} the sample standard deviation, N the number of test samples, m the Weibull modulus, and σ_0 the Weibull normalization constant.

Al_2O_3	Ni(P)	σ_f (MPa)	s_{n-1} (MPa)	N	m	σ_0 (MPa)
Rough	glycine	20	5.3	45	4.2	22.3
Rough	glycine	17	5.2	46	3.5	18.7
Rough	acetate	10	5.0	45	2.3	11.6
Rough	acetate	13	6.1	45	2.1	15.0
Smooth	glycine	47	12	47	3.9	52.3
Smooth	glycine	31	13	44	2.2	35.5
Smooth	acetate	3.7	4.9	33	0.9	3.4
Smooth	acetate	6.4	7.9	35	0.7	5.3

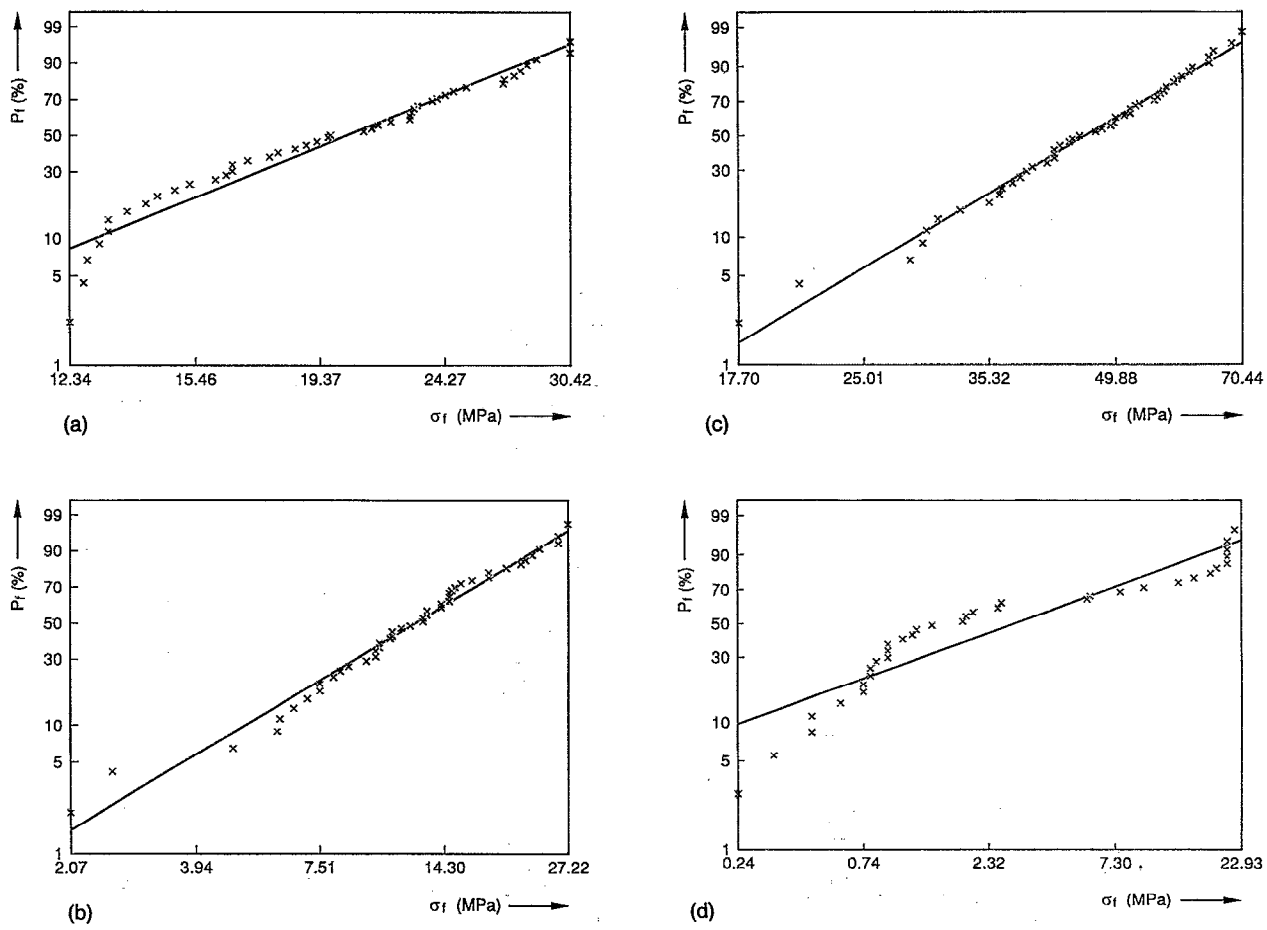

FIG. 5. Weibull plots of adhesion strength measurements: (a) sample with rough-type alumina and glycine-type Ni(P); (b) sample with rough-type alumina and acetate-type Ni(P); (c) sample with smooth-type alumina and glycine-type Ni(P); (d) sample with smooth-type alumina and acetate-type Ni(P).

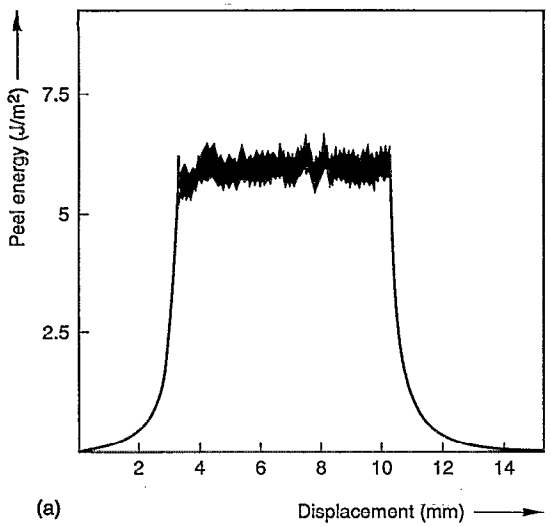

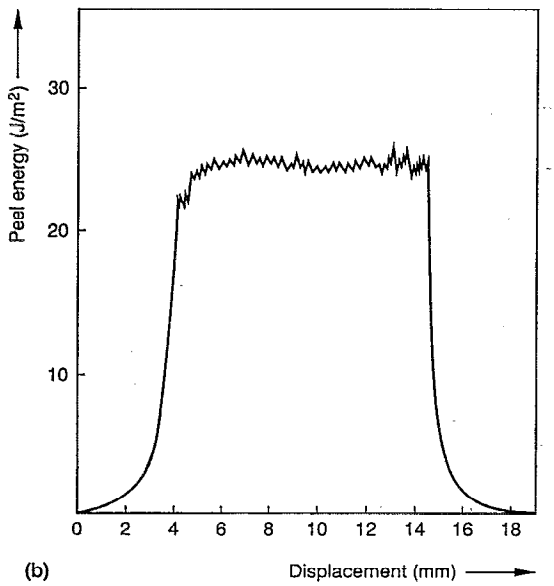

FIG. 6. (a) Peel curve of acetate-type Ni(P)-Ni layer from smooth alumina; (b) peel curve of glycine-type Ni(P)-Ni layer from rough alumina.

zero load R_p' is listed in Table III. Magnified images of peel tests were recorded on video tape. The radii were measured by fitting the images with circle segments on the monitor screen.

In Fig. 8 the load versus time is plotted by the recorder of the peel test equipment for a sample with acetate Ni(P)

TABLE II. Peel test results in which G_p is the peel energy per unit area, s_{n-1} is the sample standard deviation, and N is the number of test samples.

Al_2O_3	Ni(P)	G_p (J/m^2)	s_{n-1} (J/m^2)	N
Rough	glycine	24.3	1.63	8
Rough	acetate	40.9	4.39	8
Smooth	glycine	6.09	0.62	8
Smooth	acetate	8.45	0.25	8

TABLE III. Metal film radii during peeling R_p and after peeling R_p' for samples with various layer thicknesses T_l.

Al_2O_3	Ni(P)	T_l (μm)	R_p (mm)	R_p' (mm)	G_p (J/m^2)
Rough	glycine	11.7	0.9	3.4	23
Rough	glycine	12.5	0.8	3.5	25
Rough	acetate	10.9	0.5	1.5	42
Rough	acetate	8.3	0.4	1.2	39
Smooth	glycine	8.2	0.7	5	6.2
Smooth	glycine	7.4	0.7	4.5	6.0
Smooth	acetate	6.9	0.6	4.5	8.3
Smooth	aceteate	9.4	0.5	4.5	8.6

and a rough substrate. The peaks represent loading and unloading cycles with increasing maximum load, measured at a loading and unloading rate of 1 mm/min. This is done up to the load at which peeling starts (peak 15). For reasons of clarity only the peaks corresponding to the higher loads (peaks 10–15) are depicted in Fig. 8. The surface area under the left-hand half of the peak is linearly proportional to the amount of energy required for bending the layer. The right-hand half represents the amount of energy released elastically from the system upon unloading. If both areas are equal then the system behaves perfectly elastically. In Fig. 9 the difference between both areas (a measure of plastic deformation energy) divided by the loading area Δ is plotted versus maximum load. Within a range of 5%–10% the loading energy equals the unloading energy, up to a peel energy of about 30 J/m^2. The relative accuracy is smaller at the lower loads due to error in the surface area measurements. Only the last point in the plot, corresponding to peak 13, shows a significant deviation, which is ascribed to initiation of peeling at a small part of the peel front. Similar effects are observed at about 10% below the top load of peaks 14 and 15 in Fig. 8. Therefore, these latter peaks are not used for the plot in Fig. 9. From these measurements it can be concluded that bulk plastic defor-

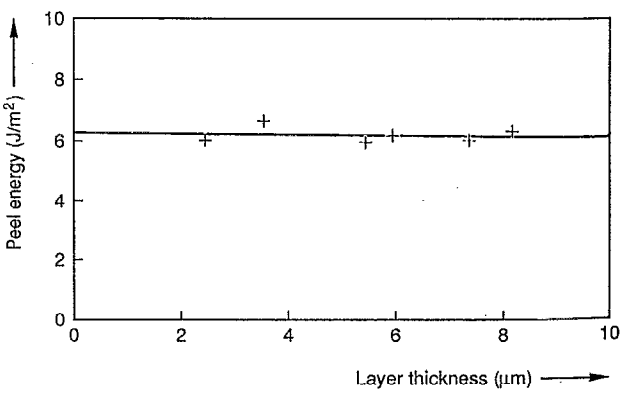

FIG. 7. Peel energy vs Ni layer thickness.

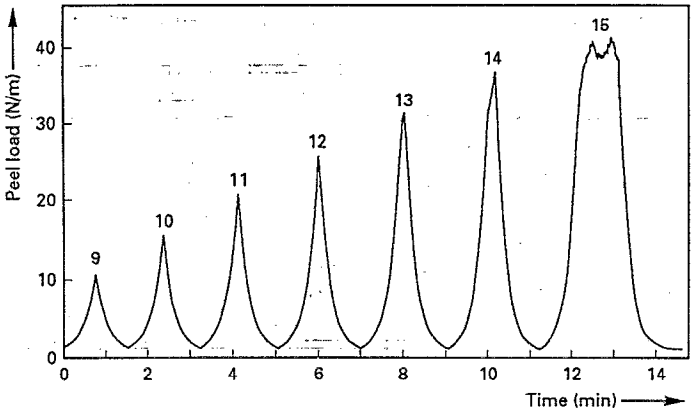

FIG. 8. Stress-strain peaks recorded in loading-unloading cycles with increasing top load. Peeling starts at peak no. 15.

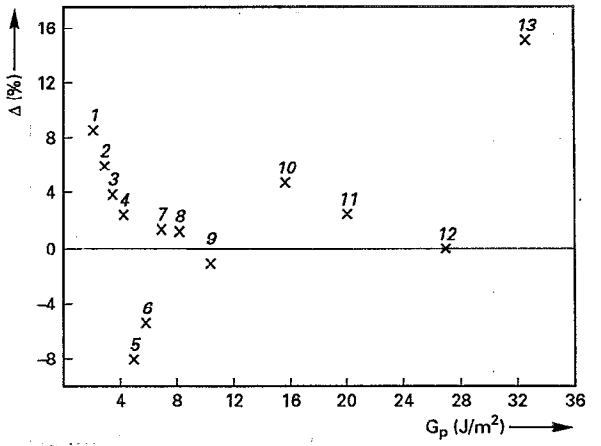

FIG. 9. Relation between elastic and plastic deformation vs load. Δ is the difference between the left-hand half of the peak areas of Fig. 6, minus the right-hand half, divided by the left-hand area.

mation of the metal film during peeling does not play an important role up to peel energies of at least 30 J/m^2. This is discussed further in Sec. V B.

C. SEM/EDX fracture surface analysis

After the strength measurements for a number of samples the fracture surfaces are analyzed by SEM and EDX in order to obtain information on the crack initiation and macroscopic (μm scale) flaws. No significant differences were observed between the fracture surfaces of the samples with acetate-type Ni(P) and with glycine-type Ni(P). Although some irregularities are observed, no clear indications of the presence of interfacial flaws are obtained for any of the samples. The metal side forms an exact replica of the substrate, and no fracture patterns can be distinguished. Samples with a strong adhesion are only fractured in the area under the stud, whereas for samples showing a weak adhesion large areas of metal film are peeled off around the pull stud. On the rough-type substrates flat areas of maximum 15 μm size are observed, where no mechanical interlocking is possible. In Figs. 10(a)–10(d) the metal and ceramic fracture surfaces are shown of samples with acetate-type Ni(P) and with both rough- and smooth-type substrates.

With EDX no Ni or P is detected on the ceramic fracture surface of the smooth-type substrates, for both the acetate-type Ni(P) and the glycine-type Ni(P). On the rough-type substrates small amounts of Ni are detected with EDX at the grain boundaries. No P is detected on these substrates. On the metal side of the fracture surfaces some Al, originating from a few detached grains, is observed on layers from rough substrates but no Al is detected by EDX for the layers which are removed from smooth substrates.

V. DISCUSSION

In this section, first the advantages and drawbacks of the DPO and peel tests for the adhesion measurement are discussed. By combining the SEM/EDX fracture surface analysis results, a good impression of the interface structure and chemical composition is obtained. The final sections deal with the mechanism of adhesion and with the relation between adhesion strength and fracture energy.

A. DPO test

1. Literature data

The strength values in the literature of Ni(P) on rough-type 96% alumina range from 10 to 30 MPa, but mostly values of about 20 MPa are reported.[7] In this work on similar substrates, values of about 12 and 18 MPa are found for acetate-type Ni(P) and glycine-type Ni(P), respectively. Since fracture energies are not reported in the literature, it is difficult to explain differences from the strength values reported here in terms of process conditions and interfacial bonding.

2. DPO test-sample preparation

The direct pull-off adhesion strength measurement procedure used in this work is slightly different from the one used in the literature.[1–6] In the procedure used in the literature first about 2 μm Ni(P) is deposited, then by photolithography flat patches of 2×2 mm^2 size are etched and a tin-plated copper wire is soldered. This procedure is more laborious than using the commercial, adhesive-coated pull studs. A few other differences from the literature method are the following: In etching there is always a risk of some degree of underetching, and the shape of a solder dot is difficult to control. With our studs a more homogeneous stress distribution is expected since bonding is axisymmetric. With soldering the wire must be accurately centered over the Ni(P) patch, while with the pull studs this is not necessary. Soldering causes a thermal shock to about 250 °C, while the studs are bonded at 160 °C. The amount of elastic strain energy is proportional to the difference in temperature squared. With the epoxy adhesive on the studs, strength values up to 80 MPa have been measured, while solder is much weaker, thus limiting the maximum measurable strength. For soldering, the Ni(P) layer thickness must at least be 2 μm because solder

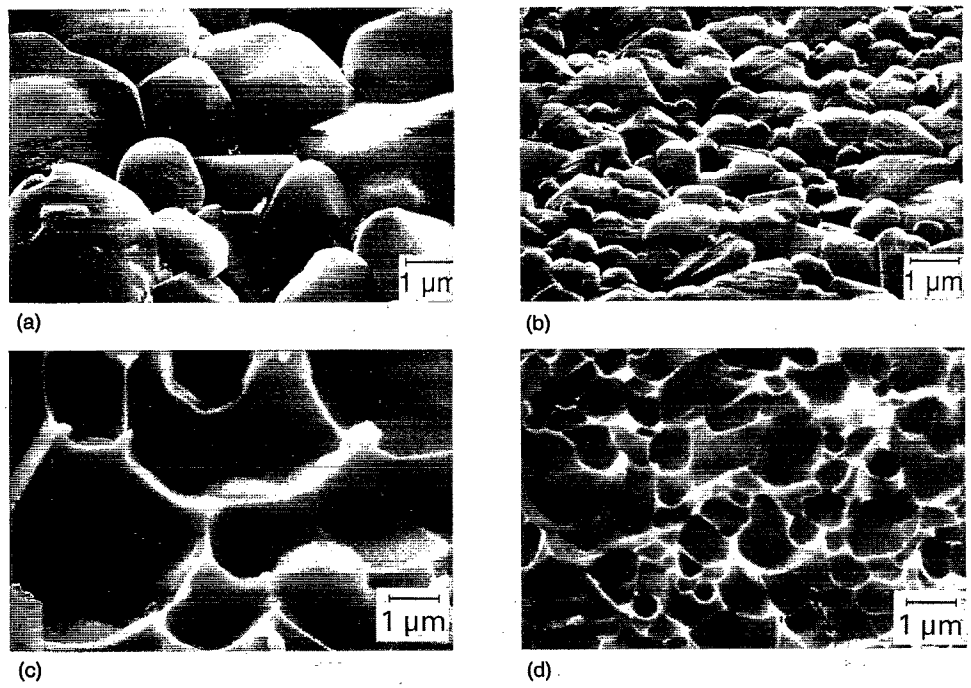

FIG. 10. SEM fractographs of samples with acetate-type Ni(P): (a) alumina side of sample with rough-type alumina; (b) alumina side of sample with smooth-type alumina; (c) Ni(P) side of sample with rough-type alumina; (d) Ni(P) side of sample with smooth-type alumina.

reacts with Ni(P). For adhesive bonding any layer thickness is suitable, if the layer is closed. In spite of the differences in adhesion strength measurement procedures, the strength values reported in the literature are of the same order as the values measured in this work.

3. Residual strain energy

In the DPO test, pull studs are bonded to the sample with an epoxy adhesive which is polymerized and solidified at 160 °C. Due to differences in thermal-expansion coefficients elastic strain energy is built up in the adhesive layer during cooling as given by Eq. (7) in Sec. II B. With an adhesive layer thickness of 10 μm and assuming purely elastic deformation (Young's modulus 1 GPa, Ref. 31), a worst-case value of the order of 0.5 J/m^2 is obtained, which is small compared to peel energies of the order of 10 J/m^2. Moreover, during or after fracture the adhesive film cannot freely expand or contract since it is restricted by the aluminum pull stud on which it remains. Therefore, it is more probable that the release of elastic strain energy is determined by the difference in thermal expansion of the aluminum pull stud and the layer-substrate combination and by the degree of relaxation of this stress by the adhesive layer during cooling. This is, however, a rather complicated mechanical problem which is not within the scope of this work. Kinloch[31] states that in most practical cases stresses are relaxed by viscoelastic deformation of the adhesive during cooling.

4. Stress concentration

As described by Kinloch,[31] stress concentration takes place at the edge of an adhesive-bonded butt-joint geometry. Consequently, in such a geometry fracture starts at the edges. In this study, due to a well-chosen nail-head-shaped pull-stud geometry [Figs. 4(a) and 4(b)], the stress at the edge is limited. For these studs the fracture was observed to start near the middle of the bonded area. (This aspect is further discussed in Sec. V C.) This is an indication that the stress at the edge does not exceed the stress at the pull-stud axis. According to Kinloch, the stress concentration is also reduced by the remaining excess adhesive at the edge, the spew fillet which can be observed in the optical micrograph in Fig. 4(b). In practice the stress is limited by viscoelastic deformation of the adhesive. An upper boundary value is given by the yield stress. Typical values for the yield stress of epoxy adhesives are in the range of 30–50 MPa.[31]

B. Peel test

1. Quantitative aspects

As discussed in Sec. I, the peel energy G_p is equal to the fracture energy G_c only if the contributions of residual strain energy G_{el} and energy of plastic deformation G_{def} are negligible [Eq. (5)]. The residual strain energy in the metal layer is proportional to the layer thickness. If this energy plays a role in the peel test, a decreasing peel energy with increasing layer thickness should have been found; however, as shown in Fig. 5, the peel energy is found not to depend on layer thickness. This can be understood by separately considering the contributions of the electrodeposited Ni layer and the electrolessly deposited Ni(P) layer to the residual strain energy. The internal stress σ_i in low-stress sulphamate Ni deposits ranges between 0 and 50 MPa.[32] Using the measured value of 40 MPa (Sec. III A) the residual strain energy G_{el} can be calculated with Eq. (8) (Sec. II B),

$$\frac{G_{el}}{T_l}=\frac{\sigma_i^2}{2E}.$$

A residual strain energy G_{el} of 0.004 J/m^2 per μm layer thickness is obtained. Therefore, it can be concluded that the residual strain energy G_{el} of the electrodeposited Ni layer does not play a significant role. Stresses in the electroless Ni(P) film depend on the phosphorus content. For a P content of about 11 wt % the stress varies between about 20 MPa tensile and 20 MPa compressive.[33] Since both the layer thickness and the internal stress are much smaller for Ni(P) than for electrodeposited Ni, the contribution of the Ni(P) layer to this residual strain energy G_{el} can be neglected as well.

In order to estimate the contribution of plastic deformation of the metal layer, the stress-strain curves were measured during loading and unloading cycles up to various top loads, lower than the peeling load as shown in Fig. 9 and as described in Sec. IV A. Since, within the experimental error, the amount of energy stored in the system during loading was completely released upon unloading, it was concluded that plastic deformation is negligible in the peel test for these samples. Therefore, the radius R_p' is caused by deformation in the plastic zone at the crack tip (see below). This is not a secondary effect, but it forms an intrinsic part of G_c (see Sec. II B). Therefore, it can be concluded that for this system the peel energy G_p is equal to the fracture energy G_c.

2. Crack-tip plasticity

Kinloch[34] found an increasing peel energy value with increasing polymer layer thickness up to several millimeters, with unaltered intrinsic adhesion. This is ascribed to the increased volume available for crack-tip plastic deformation. Owing to the much higher yield strength of metals compared with polymers, the size of the plastic deformation zone is smaller for metals. The height H of the plastic deformation zone in the metal side of the present interface (Fig. 11) is given by[34,35] (plane stress),

$$H=\frac{G_c E}{2\pi\sigma_y^2}, \tag{11}$$

in which σ_y is the yield strength of the metal phase. Using a fracture energy value G_c of 10 J/m^2, a Young's modulus of 190 GPa, and a yield strength σ_y of 400 MPa, a height H of about 2 μm results. In case of plane-strain condition the factor 2π should read 6π. In reality, a full 3D stress situation is present, for which the constant factor is somewhere between 2π and 6π. Consequently, the above estimate is a maximum estimate. It is concluded, therefore, that the height of the plastic deformation zone is not limited by the layer thickness for layer thicknesses greater than 2 μm. This is in agreement with the observation that the peel energy did not depend on the layer thickness, between 2 and 9 μm, as shown in Fig. 7.

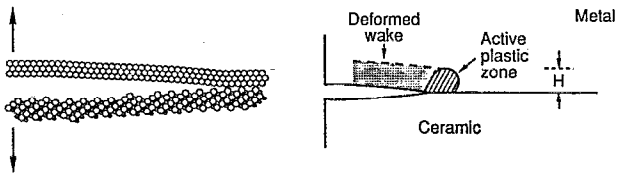

FIG. 11. Schematic representation of plastic deformation at crack tip.

3. Types of crack growth

The sawtooth structure that is observed in the peel curves of acetate-type samples is characterized as unstable brittle crack propagation.[34] The unstable, discrete nature of the crack propagation can either be explained by a strong dependence of the size of the plastic deformation zone on the crack growth rate or by a difference in intrinsic initiation and propagation fracture energies. Both phenomena result in a relatively low fracture energy at a high crack propagation rate and a high fracture energy at a low rate. When during peeling at a constant cross-head speed the crack tip advances more rapidly than the peel rate, the stress is released until fracture stops. This corresponds to a decrease in peel load. Subsequently, the peel load increases up to the higher load, corresponding with slow fracture. These higher and lower fracture energies are interpreted as initiation and arrest fracture energies, respectively. This mechanism does not, however, explain why a different, more stable crack growth is found for the glycine-type Ni(P), with fracture energies in the same range.

C. Relation between adhesion strength and fracture energy

1. Flaw size calculations

As shown by the data in Table IV there is no proportionality between interfacial fracture energy and adhesion strength, as might be expected [see Eq. (1)]. This proportionality has been observed for electrolessly deposited Ni(P) on alumina ceramic using a Ti/Pd nucleation layer.[36] Since large differences in residual stress energy due to built-in stresses or due to differences in thermal expansion would become apparent in the peel energy [see Eq. (5), Sec. II], these phenomena can be excluded as an explanation for the differences in the adhesion strength. For the calculation of critical flaw sizes a K value [Eq. (1)] of 1.13, appropriate for circular flaws, is used.[37] Even if the peel energy G_p is not equal to but only proportional to the fracture energy G_c, the trend from Table IV is clear. The highest fracture energy is measured on samples with low strength and the strongest samples have the lowest fracture energy. A wide range of interfacial flaw sizes is calculated from these values with the Griffith–Irwin equation. Since the flaw is in the proximity of the interface, an elastic modulus of the order of a few GPa, typical for the adhesive, rather than a few hundred GPa, typical for the nickel layer and the alumina substrate, has to be used. For the effective elastic modulus a value of 2 GPa is chosen. This is a different value from the Young's modulus of the epoxy

TABLE IV. Critical flaw size a_{cr} calculated from adhesion strength σ_f and fracture energy G_c values.

Al_2O_3	Ni(P)	σ_f (MPa)	G_c (J/m^2)	a_{cr} (μm)
Rough	glycine	22	24.3	120
Rough	acetate	12	40.9	700
Smooth	glycine	45	6.1	6.8
Smooth	acetate	5	8.5	730

adhesive which is used for the calculation of residual strain energy in Sec. V A (1 GPa). This difference is related to the geometry and the loading conditions. For an adhesive layer which is thin relative to its lateral dimensions and which is perfectly constrained by relatively rigid substrates, the relation between the effective modulus of the adhesive E'_a and the Young's modulus E_a under normal loading is given by[31]

$$E'_a=\frac{1-v_a}{(1+v_a)(1-2v_a)}E_a, \tag{12}$$

in which v_a is Poisson's ratio. For a Poisson's ratio of 0.35, which is a typical value for epoxy adhesives, the effective modulus may be greater than the Young's modulus by about 50%, or even more due to the spew fillet.

2. Flaw growth during testing

Flaw sizes of about 800 μm are calculated for the samples prepared with the acetate-type Ni(P), whereas for the samples with the glycine-type Ni(P) much smaller flaw sizes are obtained. In principle, there are two possibilities: Either these flaws are present at the interface after sample preparation, or they are introduced during the strength test. By scanning acoustic microscopy no indications of the presence of interface flaws are obtained from the metallized samples, within the resolution of 20 μm. Also, on the fracture surfaces no features are found which point to the presence of interface flaws. Since it is not possible to study the formation of flaws at the ceramic-metal interface during the strength measurement, polished glass plates were used as model substrates. After grinding one side was metallized and during the DPO test the interface was observed through the glass with a video camera. A sequence of photographs, shown in Fig. 12, revealed that during the strength test a flaw appears which grows in discrete steps. At a size of about 800 μm, fracture suddenly takes place.

Apparently, during this flaw formation, the Griffith–Irwin energy balance remains near to equilibrium, otherwise catastrophic failure would have taken place immediately. The possibility of slow crack growth at the interface has been considered. A peel strip with acetate-type Ni(P) was loaded with various weights, corresponding to 10%–90% of its peel load and the advance of the crack front was monitored with a camera. The peel front did not move in a week's time, not even at 90% of the peel force, within the resolution of 20–50 μm. This suggests that slow crack growth does not play an important role in these systems. Moreover, the flaw growth that was observed during the DPO test did not take place gradually but in discrete steps, while for slow crack growth a gradual increase in size is expected.

An alternative explanation for the flaw growth is related to the mechanical behavior of the adhesive layer with which the aluminum pull stud is bonded on the metal layer. The effective elastic modulus for a thin adhesive layer under normal load, with a layer thickness various orders of magnitude smaller than its lateral dimensions, is much higher than the Young's modulus [see Eq. (12)]. Only at the edges, where shear displacement in the adhesive is possible, does the effective modulus approach the Young's modulus.[38] In the vicinity of an interfacial flaw, no normal load is applied and the effective elastic modulus of the adhesive is locally reduced, limiting the amount of missing elastic strain energy, which causes catastrophic failure according to the Griffith–Irwin theory. Similar observations of a debonded area which grows during testing have been made for acrylic (Plexiglas) plates, bonded with a polyurethane adhesive.[39] It should, however, be stressed that in this case the effect is characteristic of some sample types, rather than for the DPO test. It is reasonable to assume that with smaller initial flaw sizes, this flaw growth process does not take place or takes place at higher stresses, leading more rapidly to catastrophic failure.

3. Weibull statistics

The Weibull moduli found in this work range between 0.7 and 4.2. This is relatively low compared to Weibull moduli generally found for the bulk strength of ceramics, ranging from 5 to 20.[40] In the few data that are available in the literature on Weibull moduli of adhesion strengths, the Weibull moduli for adhesion tend to be somewhat lower than for bulk strength.[41] For the joint strength of Si_3N_4/Ni-Cr systems Weibull moduli ranging from 2.3 to 6.1 were reported.[42] For both the tensile strength and the three-point bending strength of Si_3N_4/Al/Invar joints, Weibull slopes of about 6 were found.[43] For the lap shear adhesion strength of epoxy and acrylate coatings on glass a spread corresponding with a Weibull modulus of about 2 was reported.[9] By adhesion measurement with indentation for the same systems Weibull moduli of about 9 were found, which was explained by the fact that interfacial flaws do not play a role due to the small area in the indentation tests.

Generally, the distribution of flaw sizes determines the Weibull modulus value. Apparently, a wide distribution of flaw sizes is present at the interfaces studied in this work. This width may be partly explained by the stable flaw growth during testing which is described above. This growth may lead to a decreased Weibull modulus similar to that found in the case of slow crack growth.[44] This is in agreement with the observation that the lower Weibull moduli were found for samples with the largest calculated flaw sizes, viz., those with acetate-type Ni(P) (Table I). For clarity's sake it is repeated here that slow crack growth probably does not occur in our system.

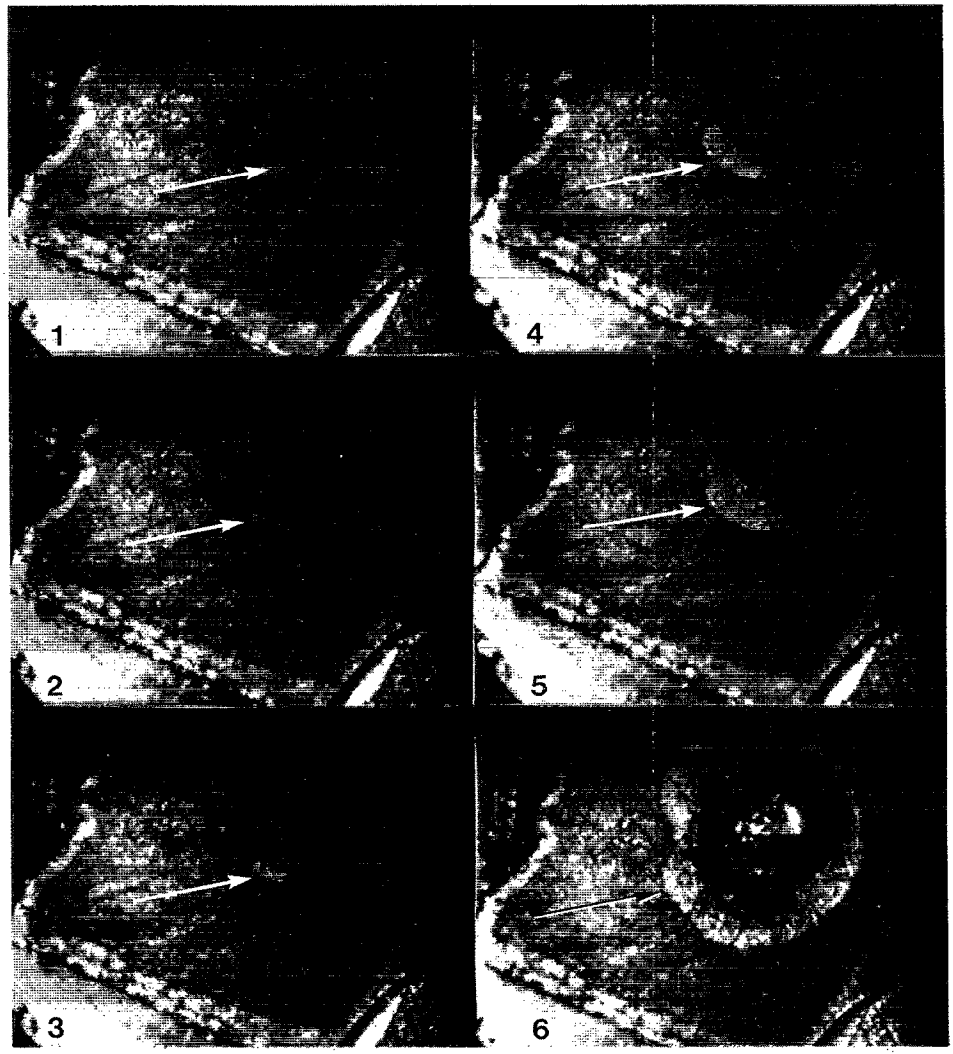

FIG. 12. Stepwise flaw growth during adhesion strength test on a glass model substrate.

VI. CONCLUSIONS

The DPO test and the peel test have been found suitable for quantitative measurement of adhesion strength and interfacial fracture energy. The Griffith–Irwin approach appeared to be an appropriate tool for the interpretation of these experiments. With a direct pull-off adhesion strength measurement, sample standard deviations of about 30% are frequently found in these measurements, for which 20–30 samples are required. Furthermore, conditions are investigated under which the 90° peel test can be used as a quantitative fracture energy measurement. By using sulphamate Ni as bulk metal layer, the influence of elastic energy stored in the layer can be neglected. This is confirmed by the observation that the peel energy is not influenced by the layer thickness. It is concluded that for the smooth substrates, the peel energy is a good approximation of the fracture energy. In the peel measurements with eight samples, standard deviations in the mean of one or a few percent are obtained.

Peel measurements show that for both the rough- and the smooth-type substrates chemical interfacial interactions contribute to the adhesion. In view of the experimental conditions it is probable that the chemical interactions are limited to van der Waals-type interactions, which is in agreement with the order of magnitude of the measured peel energies. In the companion article more information is presented on the type of chemical interactions at the interface. Only for the rough-type substrates has evidence been obtained that mechanical interlocking contributes to the adhesion. The peel measurements show that the difference in adhesion strength between the glycine-type Ni(P) and the acetate-type Ni(P) cannot be accounted for by differences in chemical or mechanical interfacial interactions or differences in residual (built-in or thermal) stresses. It is therefore concluded that the difference in adhesion strength is due to differences in interfacial critical flaw sizes. Since strong adhesion was found for samples with smooth substrates and low peel energies, it can be con-

cluded that strong adhesion can be obtained, probably by van der Waals interactions, without making use of mechanical interlocking. For most samples the adhesion strength is limited by the size of interfacial flaws. The final conclusion therefore is that further research is required to obtain insight into the origin of these flaws.

ACKNOWLEDGMENTS

Gratitude is expressed to A. van Weert and N. Sweegers for experimental assistance, W. Meerman for the design and fabrication of the peel jig, and J. Janssen (Components Roermond) for stimulating discussions.

[1] H. Honma and S. Mizushima, Kinzoko Hyomen Gijutsu **33**, 380 (1982).
[2] T. Osaka, E. Nakajima, Y. Tamiya, and I. Koiwa, Kinzoko Hyomen Gijutsu **40**, 67 (1989).
[3] T. Osaka, Y. Tamiya, K. Naito, and K. Sakaguchi, J. Jpn. Inst. Printed Circuit **4**, 285 (1989).
[4] H. Honma and K. Kanemitsu, Plating and Surface Finishing **74**, 62 (1987).
[5] T. Osaka, Y. Tamiya, K. Naito, and K. Sakaguchi, J. Surf. Finish. Soc. Jpn. **40**, 835 (1989).
[6] M. Kamijo and N. Ayuzawa, Yamanashi-ken, Kogyo Gijutsu Senta Kenkyu Hokoku, 1987, Vol. 1, p. 86. (Research report of the Yamanashi Prefectural Industrial Technology Center).
[7] J. W. Severin and G. de With, J. Adhesion Sci. Technol. **7**, 115 (1992).
[8] M. D. Thouless, Mater. Res. Soc. Symp. Proc. **119**, 51 (1988).
[9] J. E. Ritter, L. Rosenfeld, M. R. Lin, and T. J. Lardner, Mater. Res. Soc. Symp. Proc. **130**, 237 (1989).
[10] R. Jacobsson, Thin Solid Films **34**, 191 (1976).
[11] R. Jacobsson and B. Kruse, Thin Solid Films **15**, 71 (1973).
[12] P. C. Hopman, Trans. Commun. **1984**, 179.
[13] A. G. Dirks and J. J. van den Broek, Thin Solid Films **96**, 257 (1982).
[14] J. W. Severin, R. Hokke, H. van der Wel, and G. de With, J. Appl. Phys. **75**, 3414 (1994).
[15] R. J. Good, in Adhesion Measurements of Thin Films, Thick Films, and Bulk Coatings, edited by K. L. Mittal, STM STP 640, 1978, p. 63.
[16] S. J. Bennett, K. L. de Vries, and M. L. Williams, Int. J. Fracture **10**, 33 (1974).
[17] S. A. Varchenya, A. Simanovskis, and S. V. Stolyarova, Thin Solid Films **164**, 147 (1988).
[18] A. J. Kinloch, in *Adhesion and Adhesives* (Chapman and Hall, London, 1987), Chap. 3.
[19] H. F. Fischmeister, G. Elssner, B. Gibbesch, and W. Mader, Materials Research Society International Meeting on Advanced Materials **8**, 1988, p. 227.
[20] Ref. 18, Chap. 4.
[21] K. L. Mittal, J. Adhesion Sci. Technol. **1**, 247 (1987).
[22] K.-S. Kim, Mater. Res. Soc. Symp. Proc. **119**, 31 (1988).
[23] J. E. E. Baglin, Mater. Res. Soc. Symp. Proc. **47**, 3 (1985).
[24] A. N. Gent and J. Schultz, J. Adhesion **3**, 281 (1972).
[25] G. J. Lake and A. Stevenson, in *Adhesion 6*, edited by K. W. Allen (Applied Science, London, 1982), p. 41.
[26] W. Weibull, J. Appl. Mech. **18**, 293 (1951).
[27] L. J. M. G. Dortmans and G. de With, J. Am. Ceram. Soc. **74**, 2293 (1991).
[28] W. H. Safranek, *The Properties of Electrodeposited Metals and Alloys* (Elsevier, New York, 1974), Chap. 12, p. 260.
[29] Deposit stress analyser, model 683 EC, Electrochemical Co. Inc., 1600 Pennsylvania Avenue, York, PA 17404.
[30] C. H. de Minjer and P. F. J. van der Boom, J. Electrochem. Soc. **120**, 1644 (1973).
[31] Ref. 18, Chap. 6.
[32] C.-M. Lin and T.-C. Wen, Plating and Surface Finishing **78**, 70 (1991).
[33] W. Riedel, in *Funktionelle Chemische Vernicklung* (E. G. Leuze, Saulgau, 1989), p. 111.
[34] Ref. 18, Chap. 7.
[35] T. S. Oh, R. M. Cannon, and R. O. Ritchie, Mater. Res. Soc. Symp. Proc. **130**, 219 (1989).
[36] J. W. Severin, R. Hokke, H. van der Wel, M. Johnson, and G. de With, J. Electrochem. Soc. **140**, 1611 (1993).
[37] G. K. Bansal, J. Am. Ceram. Soc. **59**, 87 (1976).
[38] P. C. P. Bouten (personal communication).
[39] G. P. Anderson and K. L. DeVries, in *Treatise on Adhesion*, edited by R. L. Patrick (Marcel Dekker, New York, 1989), Vol. 6, Chap. 3, p. 102.
[40] R. W. Davidge, in *Mechanical Behaviour of Ceramics* (Cambridge University Press, Cambridge, 1979), Chap. 9, p. 136.
[41] J. T. Klomp and G. de With, Mater. Manuf. Proc. **8**, 129 (1993).
[42] S. D. Peteves, in *Ceramics Today—Tomorrow's Ceramics*, edited by P. Vincenzini (Elsevier, Amsterdam, 1991), Part B, p. 1469.
[43] K. Suganuma, T. Okamoto, M. Koizumi, and M. Shimada, J. Am. Ceram. Soc. **69**, C-235 (1986).
[44] J. D. Helfinstine, J. Am. Ceram. Soc. **63**, 113 (1980).